REVIEWS

Journal of Semiconductors
(2019) 40, 101303
doi: 10.1088/1674-4926/40/10/101303

# Perspective: optically-pumped III–V quantum dot microcavity lasers via CMOS compatible patterned Si (001) substrates

**Wenqi Wei[1], Qi Feng[1], Zihao Wang[1, 2], Ting Wang[1, 2, †], and Jianjun Zhang[1, 2]**

[1]Institute of Physics, Chinese Academy of Sciences, Beijing 100190, China

[2]Center of Materials Science and Optoelectronic Engineering, University of Chinese Academy of Sciences, Beijing 100049, China

**Abstract:** Direct epitaxial growth III–V quantum dot (QD) structures on CMOS-compatible silicon substrates is considered as one of the most promising approaches to achieve low-cost and high-yield Si-based lasers for silicon photonic integration. However, epitaxial growth of III–V materials on Si encounters the following three major challenges: high density of threading dislocations, antiphase boundaries and thermal cracks, which significantly degrade the crystal quality and potential device performance. In this review, we will focus on some recent results related to InAs/GaAs quantum dot lasers on Si (001) substrates by III–V/IV hybrid epitaxial growth via (111)-faceted Si hollow structures. Moreover, by using the step-graded epitaxial growth process the emission wavelength of InAs QDs can be extended from O-band to C/L-band. High-performance InAs/GaAs QD microdisk lasers with sub-milliwatts threshold on Si (001) substrates are fabricated and characterized. The above results pave a promising path towards the on-chip lasers for optical interconnect applications.

**Key words:** quantum dots; silicon photonics; epitaxial growth; semiconductor lasers

**Citation:** W Q Wei, Q Feng, Z H Wang, T Wang, and J J Zhang, Perspective: optically-pumped III–V quantum dot microcavity lasers via CMOS compatible patterned Si (001) substrates[J]. *J. Semicond.*, 2019, 40(10), 101303. http://doi.org/10.1088/1674-4926/40/10/101303

## 1. Introduction

With the increasing demand of datacenter and cloud-based applications, large-scale optoelectronic integration is considered as one of the most promising approaches to meet the requirements. By taking advantages of CMOS foundries, silicon photonic technologies are recognized as a major step towards monolithic optoelectronic integration, which has attracted significant attentions[1–3]. Moreover, in the past decades, tremendous progresses have been made in the development of silicon photonic devices such as waveguides[4, 5], detectors[6, 7], modulators[8, 9], and multiplexers/demultiplexers[10]. However, low-cost, high-yield and reliable integrated silicon-based on-chip lasers with emission wavelength at both 1300 nm (O-band) and 1550 nm (C/L-band) are still absent, remaining as the biggest obstacle to realize the large-scale optoelectronic integration[11]. Much efforts have been made to achieve high-performance silicon-based lasers and impressive breakthroughs about group IV lasers have been obtained in recent years[12–14]. Unfortunately, due to the indirect bandgap nature of group IV materials, group IV lasers have an inefficient radiative recombination which will block lasing[11]. As a contrast, III–V QD lasers integrated on Si substrates are believed to be the optimal solution for the integrable on-chip light source because of their superior optical and electrical properties. In addition, III–V QD lasers have a high stability, low threshold current density, and insensitivity to defects and temperature, which make them the best candidates as the on-chip light sources[15]. As a result, significant attentions have been paid to the monolithic integration of III–V QD lasers on Si substrates. In the last two decades, the wafer-bonding (flip-chip bonding) techniques have been well investigated for III–V/Si integration towards industrial applications[16, 17]. However, rising bonding and alignment costs lead to incapability of large-scale optoelectronic integration. It is natural that direct epitaxial growth III–V lasers on Si substrates is deemed to be a promising approach for cost-effective and high-volume integration of photonics integrated circuits (PICs)[18, 19].

To realize monolithic epitaxial growth of III–V laser structures on Si substrates, three critical issues must be solved, referring to the materials' large lattice mismatch, polarities differences and thermal expansion coefficients contrast between III–V epi-layers and group IV substrates.

As shown in Fig. 1(a), the existence of approximately 4% (7.5%) lattice mismatch between GaAs (InP) and Si[20], normally leads to the generation of high defect density in the order of $10^9$–$10^{10}$ cm$^{-2}$. Fig. 1(b) shows a typical cross-sectional transmission electron microscopy (TEM) image of the interface between GaAs and Si substrate, where high density of dislocations can be observed clearly. Moreover, high density of threading dislocations (TDs), which will propagate along the growth direction of III–V epi-layers and degenerate the quality of III–V materials and devices' performance[21], can be found in the upper region of III–V buffer layers. To reduce the TDs of GaAs/Si hybrid growth, various techniques have been conducted, such as implementing multilayers of InGaAs/GaAs strained-layer superlattices (SLSs), InAlAs/GaAs SLSs and InAs/GaAs QD structures as dislocation filter layers (DFLs)[22, 23]. After several periods of DFLs, the defect density can be significantly reduced to the order of $10^6$ cm$^{-2}$[23].

Correspondence to: T Wang, wangting@iphy.ac.cn
Received 13 JULY 2019; Revised 9 SEPTEMBER 2019.
©2019 Chinese Institute of Electronics

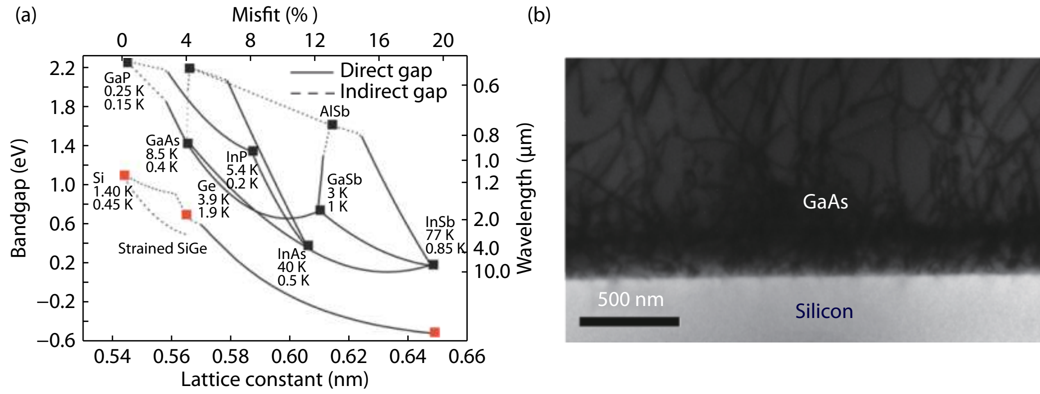


Fig. 1. (Color online) (a) The plot of bandgap energy and wavelength versus lattice constant and misfit between III–V and group IV [20]. The electron and hole mobilities in units of $cm^2/(V{\cdot}s)$ are also shown below the chemical symbols. (b) Cross-sectional TEM image on the interface between GaAs and silicon.

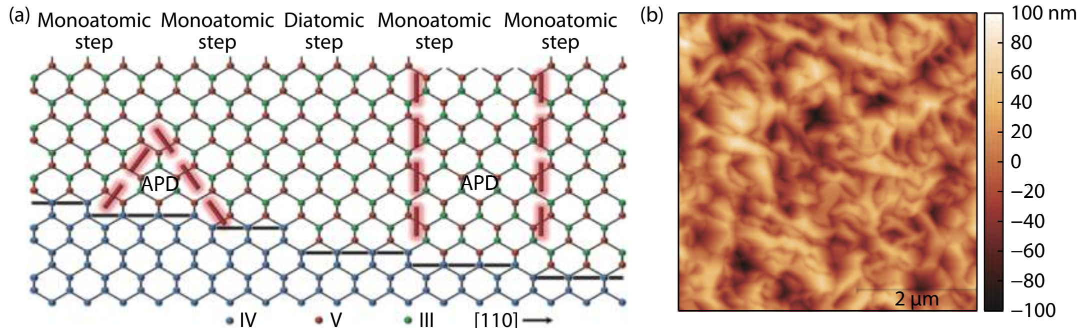


Fig. 2. (Color online) (a) Schematic showing polar/nonpolar interface between GaAs and Ge. Mono-atomic steps on Ge surface result in APBs, planes of As–As or Ga–Ga bonds. The antiphase domains (APBs) can also self-annihilate (left) or rise to the epi-layer surface (right). Diatomic steps on the Ge surface (center) do not result in APB formation[25]. (b) Surface AFM image of GaAs grown on Si (001) substrate, which indicates a high density of APBs.

As mentioned above, when the III–V materials with polar bonds are grown on non-polar group IV substrates, due to the existence of monoatomic steps on the group IV substrates, the antiphase boundaries (APBs) occur[24–26]. Fig. 2(a) shows the schematic diagram related to the formation of APBs during the growth of GaAs layer on the nonpolar Ge substrate. When the APBs rise to the material surface, they can be clearly observed by atomic force microscopy (AFM) measurement. Fig. 2(b) displays an AFM image of GaAs epitaxy on an exact Si (001) substrate by solid-source MBE, showing a rough surface full of irregular and curved boundaries. The APBs, acting as non-radiative recombination centers, are electrically charged planar defects in optoelectronic devices and leakage paths in electronic devices. The optical properties of APBs on III–V layers can be characterized by photoluminescence (PL) quenching and spectral broadening[27, 28], while the electrical properties of APBs can be manifested by the significantly degraded electron mobility[28, 29]. In order to avoid formation of APBs, several approaches have been utilized. Initializing Si substrate with a 4°–6° offcut towards the [110] direction, single atomic steps prefer to reorganize into energetically more stable double steps under a high temperature annealing condition[30]. As a result, the APBs can be minimized or eliminated. Since the first demonstration about electrically pumped high performance 1.3 $\mu$m InAs/GaAs QD laser on an offcut Si substrate by Wang *et al.*[31], extensive studies have been conducted to realize III–V QD lasers on offcut Si substrates[32, 33]. However, the offcut Si substrates are not a standard platform for silicon photonic integration, realizing high-performance III–V QD lasers on CMOS-compatible Si (001) substrates becomes an ultimate goal for on-chip light sources. So far, notable achievements on III–V QDs lasers on exact Si (001) substrates by various approaches have been made, such as by use of V-grooved Si patterned substrates, commercialized exact GaP/Si (001) substrates, or direct epitaxial growth with special surface treatment[34–39].

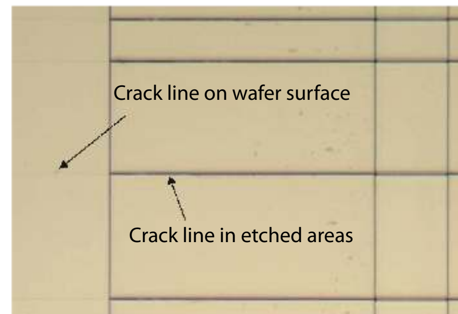


Fig. 3. Optical microscope image of the thermal cracks on III–V/Si surface.

Due to the different thermal expansion coefficients between III–V and group IV materials (Si: $2.59 \times 10^{-6}$ $K^{-1}$, GaAs: $5.73 \times 10^{-6}$ $K^{-1}$), the thermal stress will accumulate in the thick III–V epi-layer when the wafer is cooled down from high growth temperature to room temperature, which will lead to formation of thermal micro-cracks (see Fig. 3) to re-

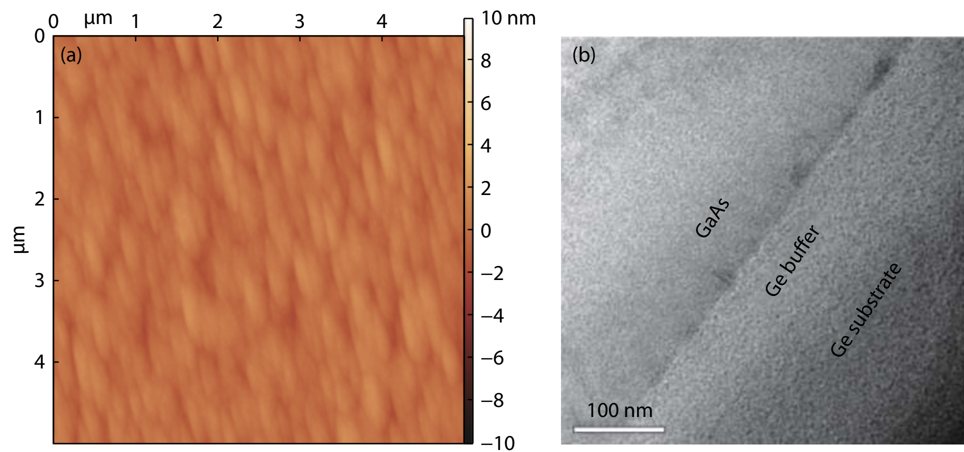


Fig. 4. (Color online) (a) 5 × 5 $\mu$m$^2$ AFM image of 250 nm GaAs buffer layer epitaxial growth on Ge substrate. (b) Cross-sectional TEM image at the interface of GaAs and Ge.

lieve the thermal stress. The thickness of III–V epi-layer and the change of wafers' temperature ($\Delta T$) both have an important influence on the formation of thermal micro-cracks. Critical thickness of the crack formation on GaAs epi-layer on Si to be experimentally observed is approximately 7 $\mu$m for a $\Delta T$ of 575 °C, 5.1 $\mu$m for a $\Delta T$ of 675 °C, and 4.9 $\mu$m for a $\Delta T$ of 725 °C[24, 40].

## 2. Hetero-epitaxial growth of III–V QDs on Ge and (111)-faceted Si (001) substrates

As stated above, to realize the low-cost, high-yield, reliable and epitaxially grown Si-based III–V QD laser for Si photonics integration, the three major obstacles must be overcome. The progress of highly efficient O-band and C/L-band wavelength emission of InAs QDs on both Ge and Si substrates[41–43] are discussed in details below.

### 2.1. InAs QDs on Ge substrates

The first InAs QD laser with ultra-high performance on Ge substrate was reported in the year of 2011 by Liu *et al.*[44], following with many demonstrations of III–V QD laser on offcut Si and Ge-on-Si substrates by direct epitaxy[31–33]. Ge is compatible with the standard CMOS process, and moreover, the fabrication of Ge-on-Si virtual substrates has becoming mature in recent years. Here, we have achieved ultra-thin growth of III–V materials on Ge substrate by a solid-source MBE[41].

Comparing to the work reported previously[44], in which approximately 1.5 $\mu$m thick III–V buffer layers on offcut Ge is required, we use only 250 nm thick GaAs buffer layer to obtain APB-free and highly smooth GaAs/Ge substrates. A Ge (001) substrate with 2° offcut towards [110] orientation was used to prevent the formation of APBs. First, the offcut Ge substrate was deoxidized at 450 °C for about 15 min before the Ge homoepitaxial growth. Then the substrate was cooled down to 300 °C for the following 60 nm Ge growth. Then it was followed by an *in-situ* annealing process at an optimized temperature of 540 °C for 90 min to obtain double atomic steps on Ge surface. For the subsequent GaAs heteroepitaxial growth, migration enhanced epitaxy (MEE) and two-step growth processes are adopted to get high-quality GaAs layer with thin thickness. The MEE layer was grown at 360 °C and the two-step GaAs growth consisted of 20 and 230 nm at 450 and 560 °C, respectively. Fig. 4(a) shows the 5 × 5 $\mu$m$^2$ AFM image of 250 nm GaAs buffer layer epitaxial growth on Ge substrate, which has a root-mean-square (RMS) of 0.57 nm. An APB-free and flat GaAs buffer layer was grown on Ge substrate. Fig. 4(b) is the cross-sectional TEM image of interface between GaAs and Ge buffer. It clearly shows that low-density defects are mostly localized at the interface region.

Based on the high quality and ultra-flat GaAs layer on Ge substrate, a standard O-band structure with five-layer InAs/GaAs dot-in-a-well (DWELL) was grown at 450 °C. It is identical to those optimized structures grown on GaAs substrate. The schematic of the structure is shown in Fig. 5(a). Here, each DWELL layer consists of a 6-nm $In_{0.14}Ga_{0.86}As$ capping layer, a 3.1-monolayer (ML) InAs QD layer and a 2-nm $In_{0.14}Ga_{0.86}As$ wetting layer. The capping layer and wetting layer were grown at 450 °C. The 50 nm GaAs spacer layers were grown at an optimum temperature of 560 °C between each InAs/GaAs DWELLs. The room-temperature (RT) PL spectra were shown in Fig. 5(b), which indicate similar PL intensity can be obtained on both GaAs/Ge substrate and GaAs substrate. High quality five-layer DWELL structure with defect free can be obtained, with a dot density of 3.6 × $10^{10}$ cm$^{-2}$, as shown in the zoomed-in TEM image in the inset.

Since most of passive and active devices for Si photonics are based on C-band long-haul telecommunications, III–V light sources on Si at 1.55 $\mu$m are becoming strongly demanded. It is believed that the Si-based high-gain III–V semiconductor optical amplifiers (SOAs) at C/L-band are essential components for the long-haul transmission[45]. In order to achieve C/L-band emission of InAs QDs on the GaAs/Ge substrate, we utilized the step-graded metamorphic InGaAs buffer layers[46]. It is the first time to realize RT C/L-band light source of InAs QDs epitaxially grown on Ge substrate[41].

For the growth of InGaAs metamorphic buffer layer on GaAs/Ge substrate, step-graded epitaxial growth method and cycle annealing process were both conducted to get high-quality InGaAs layers. First, a step-graded InGaAs layer of the thickness of 200 nm from $In_{0.09}Ga_{0.91}As$ to $In_{0.13}Ga_{0.87}As$ was deposited on GaAs/Ge substrate, followed by a 200 nm $In_{0.13}Ga_{0.87}As$ layer, which were both grown at 380 °C. Then, another step-graded InGaAs layer from $In_{0.13}Ga_{0.87}As$ to $In_{0.25}Ga_{0.75}As$ was deposited at 380 °C, followed by a 100 nm $In_{0.25}Ga_{0.75}As$ layer grown at 500 °C. To further reduce the defect density, the wafer was annealed at 500 °C for 30 min adja-

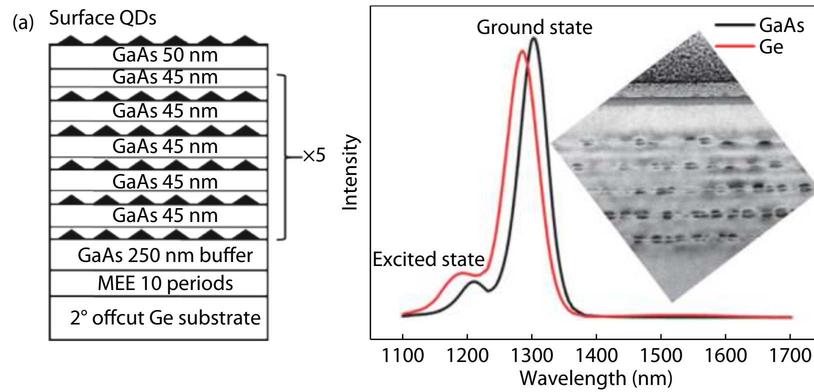


Fig. 5. (Color online) (a) The schematic of 5-layer InAs/GaAs QD structure grown on Ge substrate for O-band wavelength emission. (b) RT PL spectra of InAs/GaAs QDs on GaAs/Ge substrate and GaAs substrate, respectively. Inset: Zoomed-in cross-sectional TEM image of InAs/GaAs QDs on GaAs/Ge substrate.

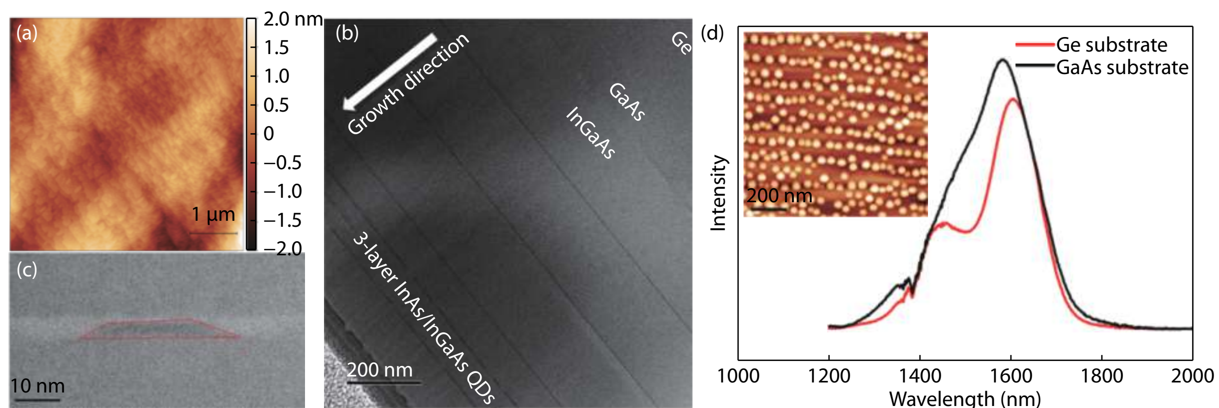


Fig. 6. (Color online) (a) 5 × 5 $\mu$m$^2$ AFM image of InGaAs metamorphic buffer layer epitaxially grown on GaAs/Ge substrate. (b) The cross-sectional TEM image of the epitaxial structures on Ge. The arrow shows the growth direction. (c) High-magnification TEM image of a truncated InAs/InGaAs QD. (d) RT PL spectra of InAs/InGaAs QDs grown on both Ge substrate and GaAs substrate. Inset: 1 × 1 $\mu$m$^2$ AFM image of InAs QDs on Ge substrate.

cently after each growth of InGaAs buffer layer of 200 nm thick. As the 5 × 5 $\mu$m$^2$ AFM image shows in Fig. 6(a), a flat $In_{0.25}Ga_{0.75}As$ metamorphic buffer layer was achieved on GaAs/Ge substrate with a 0.45 nm RMS.

The active region consisting of 3 periods of InAs QD layer was grown on the flat top and high quality $In_{0.25}Ga_{0.75}As$ buffer layer. Each InAs QD layer was made up of 2.8-ML InAs capped by a 4 nm $In_{0.25}Ga_{0.75}As$, which were both grown at 465 °C. The 45 nm $In_{0.25}Ga_{0.75}As$ spacer layers used to separate the InAs QD layers were grown at an optimized temperature of 500 °C. Cross-sectional TEM characterization of the whole structure was conducted, and it is presented in Fig. 6(b). Fig. 6(c) shows the high-magnification TEM image of a truncated InAs/InGaAs QD. Moreover, PL measurements of InAs/InGaAs QDs on both Ge and GaAs substrates were characterized, and normalized RT PL spectra are shown in Fig. 6(d). The PL intensity of InAs/InGaAs QDs on Ge substrates at C/L-band wavelength is about 85% of that on GaAs substrates. The 1 × 1 $\mu$m$^2$ AFM image of InAs QDs on Ge substrate is shown in the inset of Fig. 6(d), with a dot density of 2.55 × $10^{10}$ cm$^{-2}$. More details can be found in Ref. [41].

### 2.2. InAs QD monolithically grown on (111)-faceted Si (001) substrates

Although many works on 1300 nm InAs QD lasers have been reported on offcut Ge and Si substrates[31–34, 45, 47–51], significant attentions have been paid to the InAs QD lasers on on-axis Si substrate due to the compatibility to the mature Si microelectronics technology[34–39, 52, 53]. In 2015, Lau *et al.* reported the first defect-free GaAs film grown on V-grooved Si (001) substrates using the selective aspect ratio trapping (ART) concept by metal oxide chemical vapor deposition (MOCVD)[54]. By utilizing these specially designed V-grooved Si structures, although almost all the APBs and lattice-mismatch induced dislocations can be confined at the interface of III–V/Si, there is still remaining issue with thermal-crack generation. In the following part, a novel (111)-faceted silicon hollow substrate[42] will be discussed to solve the three big problems of III–V epitaxy on Si substrate for improving the quality of laser structure.

U-shaped pattern with ridges along [110] direction on standard 8-inch Si (001) wafers were prepared as following: 1) $SiO_2$ deposition as hard mask, 2) U-shape pattern by deep ultraviolet (DUV) photolithography, 3) dry etching, and 4) removal of $SiO_2$ in a diluted hydrofluoric acid (HF) solution. As shown in Fig. 7(a), a period of 360 nm with a 140 nm width ridge and a 500 nm depth groove in the U-shape pattern is achieved following the process described above. 3.2 × 3.2 cm$^2$ dies can be obtained by cleaving this 8-inch wafer. After *ex-situ* chemical cleaning, and oxide layer removal in a

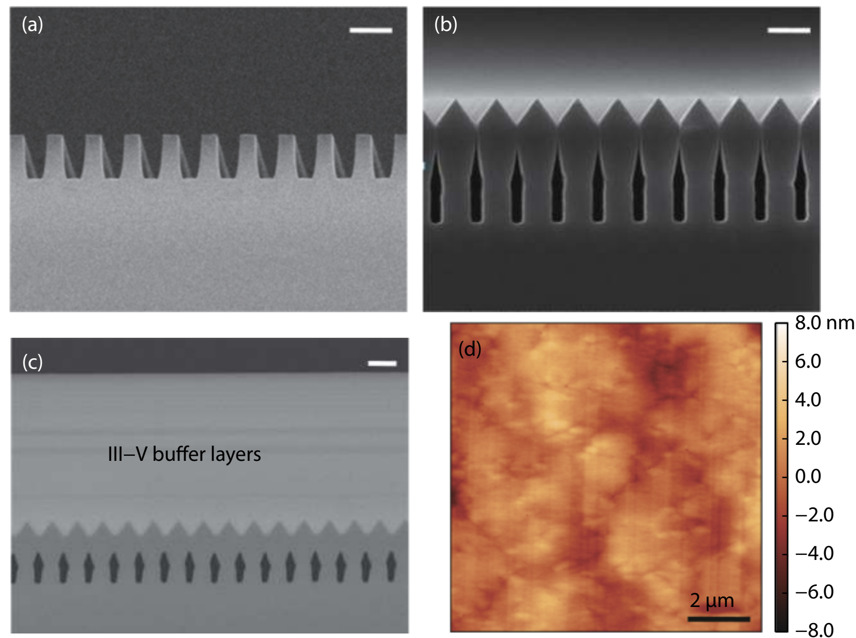


Fig. 7. (Color online) (a), (b) and (c) Cross-sectional SEM images of U-shape patterned Si substrate, homoepitaxy of 550 nm Si on (111)-faceted Si hollow substrate, and III–V buffer layers on (111)-faceted Si hollow substrate, respectively. All the images are taken along the [110] axis. (d) 10 × 10 $\mu m^2$ AFM image of III–V buffer layers on Si substrate.

diluted HF solution, the patterned Si substrate was loaded into SiGe MBE chamber and heated up to 720 °C for outgassing. Then homoepitaxy of 550 nm Si layer was conducted at a growth rate of 1.0 Å/s at 600 °C. After that, the (111)-faceted Si hollow structures were achieved on the U-shape patterned Si (001) substrate, as shown in Fig. 7(b). The Si substrate with hollow structures was then transferred to the III–V MBE chamber for the following hybrid growth. Fig. 7(c) shows the SEM image of III–V buffer layer on (111)-faceted Si hollow substrate. Owing to the novel (111)-faceted structures, the APBs and dislocation defects can be confined at the III–V/Si (111) interface. More importantly, the thermal stress during the temperature change of substrates can benefit from this hollow structure.

The GaAs buffer layers were deposited by using a two-step method consisting of a 40-nm-thick buffer layer grown at 380 °C and a 560-nm-thick buffer layer grown at 580 °C. To note, before the main GaAs layers, a 10-nm-thick AlAs layer was deposited on the (111) facets as a nucleation layer at a growth rate of 0.5 Å/s, which can significantly reduce the defect density at the III–V/Si interface due to the higher bonding energy of AlAs[51]. To further decrease the defect density, two repeats of InGaAs/GaAs QWs as DFLs separated by GaAs spacing layers of 200 nm thick were grown at 480 °C. In addition, InAlAs/GaAs DFLs were grown at 480 °C, which were effective to filter the TDs[23]. Finally, five periods of GaAs/AlGaAs superlattices (SLs) separated by 50 nm GaAs spacing layers were grown at 580 °C in order to obtain a smooth GaAs surface. Fig. 7(d) shows a 10 × 10 $\mu m^2$ AFM surface image with RMS of 1.3 nm after the whole III–V buffer layers epitaxy on Si substrate, indicating a smooth GaAs buffer on Si (001) was achieved.

The cross-sectional TEM, electron channeling contrast imaging (ECCI), and plan-view TEM measurements were carried out to verify the quality of GaAs layers on Si (001). Cross-sectional TEM image taken along [110] axis of GaAs on (111)-faceted Si hollow substrate is presented in Fig. 8(a). It shows that most of the defects are confined at the III–V/Si interface. In addtion, the defects propagate into the upper region lying on (111) planes, and they will merge at the tip of saw-tooth structures and then annihilate. This is due to the high symmetry and uniformity of homoepitaxially formed Si saw-tooth structures. InGaAs/GaAs DFLs could then completely filter some propagating dislocations. Moreover, the EECI and plan-view TEM results shown in Fig. 8(b) and Fig. 8(c) show that a low defect density (ECCI: 4.8 × $10^6$ $cm^{-2}$, and plan-view TEM: 7.0 × $10^6$ $cm^{-2}$) was observed on the surface of GaAs/Si (001). By means of these specially designed Si (001) substrates and hybrid epitaxy method, high-quality and smooth GaAs layers can be achieved on on-axis Si (001) substrate, which serves as an essential platform for integration of III–V photonic structures on Si (001) substrates.

On the high-quality GaAs/Si (001) platforms, the 1300 and 1550 nm InAs QD structures are grown, respectively. The standard five-layer InAs/GaAs DWELL structure was grown on GaAs/Si (001) substrate for the 1300 nm wavelength emission. The material growth details can be found in section 2.1. More importantly, although there is some work about lasers on Si with C/L-band telecom window emission[55–58], the use of complex phosphide-based structures will increase the difficulty for device fabrication and further on-chip integration. Here, to extend the emission wavelength to C/L-band, InGaAs metamorphic buffer layer was utilized on GaAs/Si (001) substrates as those on GaAs/Ge substrates, as described previously. The step-graded growth method and cycle annealing process were utilized to get high-quality and flat $In_{0.25}Ga_{0.75}As$ on GaAs/Si (001) substrates. Then 5-layer $InAs/In_{0.25}Ga_{0.75}As$ QD active region was deposited on InGaAs/GaAs/Si (001) substrates. Finally, $InAs/In_{0.25}Ga_{0.75}As$ QDs at surface were epitaxially grown with the same growth condition as the buried $InAs/In_{0.25}Ga_{0.75}As$ QDs, for AFM characterization.

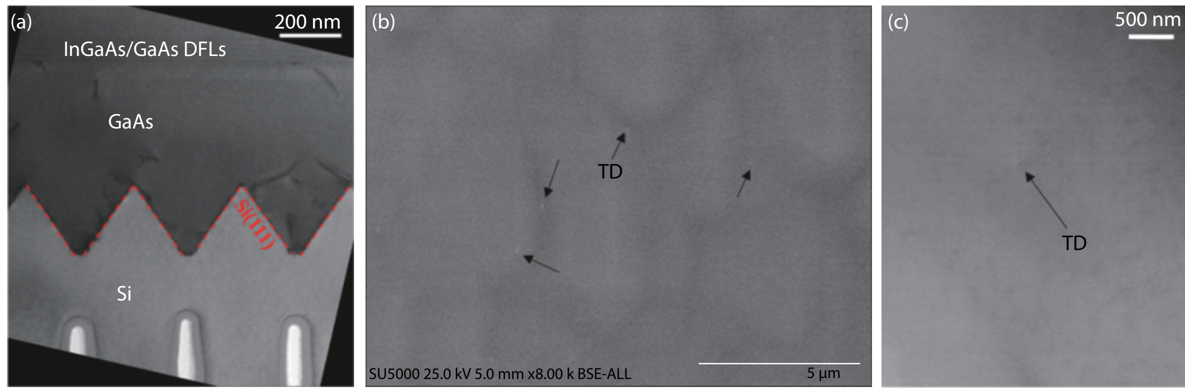


Fig. 8. (Color online) (a) Cross-sectional TEM image of GaAs on (111)-faceted Si hollow substrate, taken along [110] axis. (b) Plan-view ECCI to show TDs on GaAs/Si template. (c) Plan-view TEM image of GaAs surface on Si.

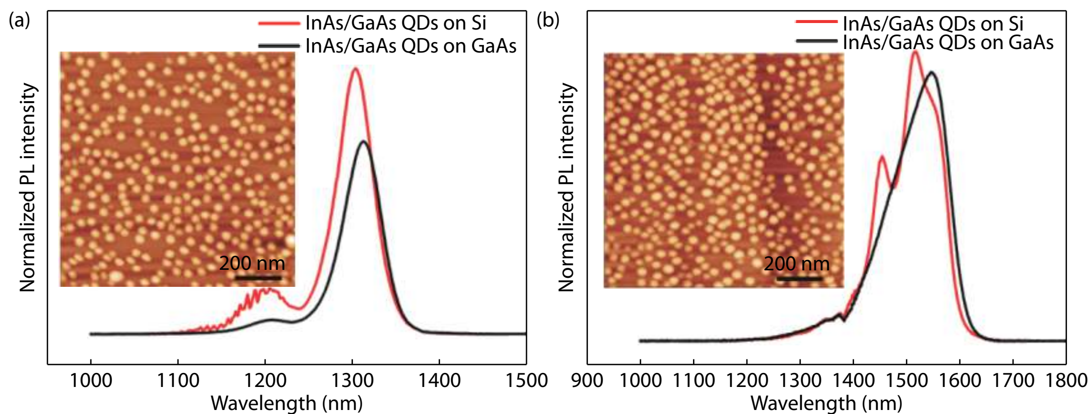


Fig. 9. (Color online) (a) RT PL spectra of InAs/GaAs QDs grown on both GaAs and GaAs/Si (001) substrates, for O-band emission. Inset: 1 × 1 $\mu$m$^2$ AFM image of InAs/GaAs QDs on GaAs/Si substrate. (b) RT PL spectra of InAs/InGaAs QDs grown on both GaAs and GaAs/Si (001) substrates, for C/L-band emission. Inset: 1 × 1 $\mu$m$^2$ AFM image of surface InAs/InGaAs QDs on GaAs/Si substrate.

The PL measurements at room temperature of InAs/GaAs and InAs/InGaAs QDs on both GaAs substrates and GaAs/Si substrates were carried out, and PL spectra at O-band and C/L-band are both shown in Fig. 9. Fig. 9(a) shows typical PL emission at 1300 nm with a FWHM of 36 meV from InAs/GaAs QDs on GaAs/Si (001) substrates. It is suggested that the stronger peak intensity in PL spectrum on Si substrate may result from the enhanced pump power from bottom grating-like (111)-faceted Si structures[42, 43, 59]. The inset in Fig. 9(a) shows a 1 × 1 $\mu$m$^2$ AFM image of surface InAs/GaAs QDs on GaAs/Si substrate with the density of 3.3 × $10^{10}$ cm$^{-2}$. In addition, a stronger peak intensity is also found on GaAs/Si (001) than that on GaAs substrate for the C/L band emission, as shown in Fig. 9(b). The multiple peaks can be observed for C/L band emission, which might be attributed to the non-uniformity of QD sizes shown by the 1 × 1 $\mu$m$^2$ AFM image in inset of Fig. 9(b). The PL intensity of C/L-band InAs/InGaAs QDs on GaAs/Si (001) substrate is approximately one third of that from O-band InAs/GaAs QDs on GaAs/Si (001) substrate, which paves the way for realization of highly efficient and integrated InAs QD lasers at C/L-band on exact Si (001) substrate in the near future.

In summary, highly efficient O-band and C/L-band emission of InAs QDs monolithically grown on CMOS-compatible Si (001) substrates have been achieved by using (111)-faceted Si (001) hollow structures via a dual-chamber *in-situ* hybrid growth method. More importantly, the (111)-faceted Si (001) hollow structures can release the thermal stress between III–V epitaxial layers and Si substrate in a certain extent. This growth method enables the possibility of fabricating high yield and performance III–V optoelectronic devices covering the two communication windows (1300 and 1550 nm) on CMOS-compatible Si (001) substrates.

## 3. Optically pumped 1300 nm InAs QD micro-disk lasers on (111)-faceted Si (001) susbtrates

Due to the advantages of high quality-factor, small footprint, and low power consumption[60], the microdisk laser is considered as a promising candidate of light sources for the low-cost and compact photonic integrated circuits (PICs) on silicon platform. Although some researches have been reported about 1300 nm InAs QD microdisk lasers on Si substrate recently[54, 61–63], the reliable, low-cost, and compact microdisk lasers with high performance are still the focus of the large-scale optoelectronic integration. By using the high-quality GaAs/Si (001) platforms stated above, we also grew and fabricated the optically pumped InAs QD miscrodisk lasers. The materials growth and fabrication process will be discussed as below.

We have demonstrated the high-quality GaAs layers on (111)-faceted Si (001) hollow substrate without defects, APBs, and thermal cracks. The microdisk laser structures were grown on these GaAs/Si (001) platforms, which consisted of a 600 nm $Al_{0.7}Ga_{0.3}As$ sacrificial layer and a 700 nm disk region.

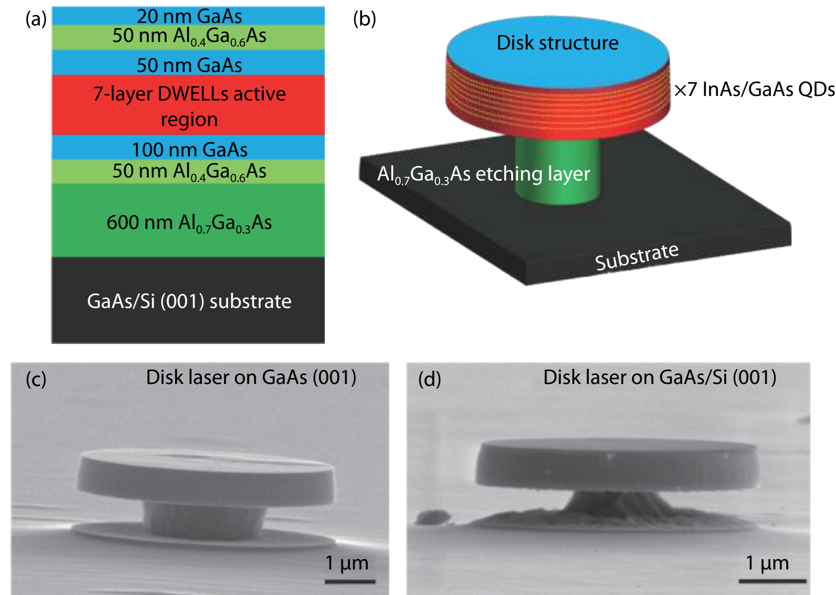


Fig. 10. (Color online) Schematic diagrams of (a) microdisk laser structure and (b) microdisk laser on GaAs/Si (001) substrate. (c) and (d) Tilted SEM images of microdisk lasers on GaAs (001) and GaAs/Si (001) substrates, respectively.

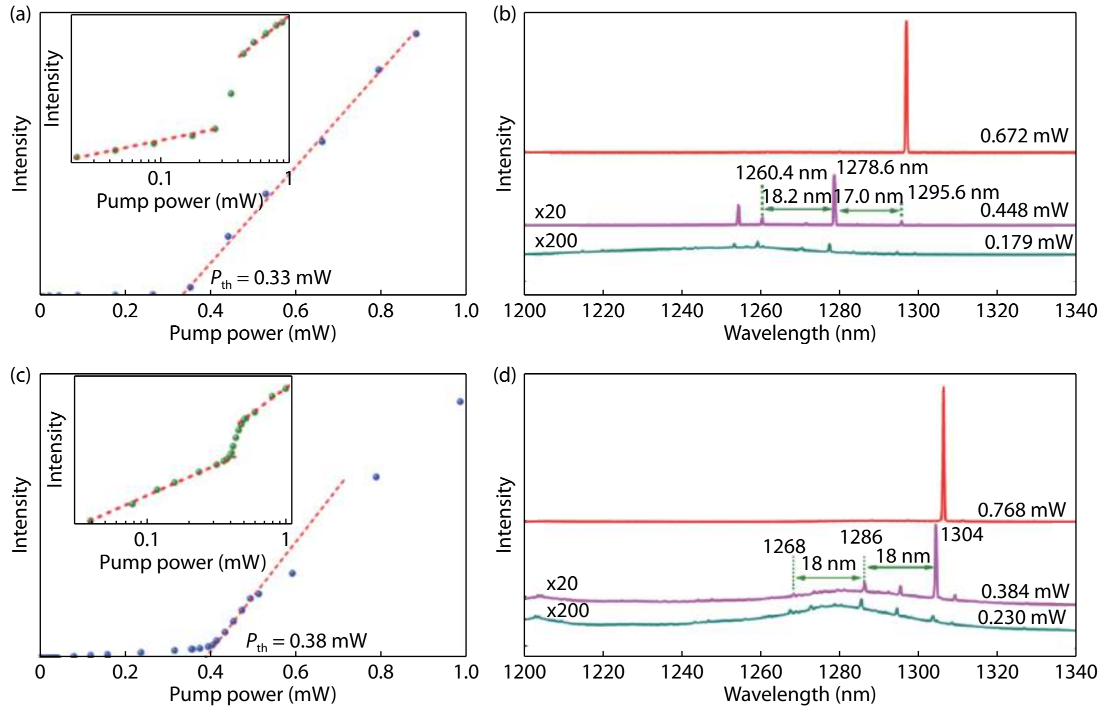


Fig. 11. (Color online) Integrated intensity of microdisk lasers versus the power of pump laser on (a) GaAs substrate and (c) Si (001) substrate, respectively. Inset: the log–log plot of 'L–L curve'. PL spectra of microdisk lasers on (b) GaAs substrate and (d) Si (001) substrate, respectively, under different pump powers.

The active region consists of a 7-layer InAs DWELLs, and the DWELL structure was grown at the same condition as described in section 2.1. At last, 50 nm thick $Al_{0.4}Ga_{0.6}As$ layer was deposited to enclose the active region as a barrier. Moreover, a reference sample on standard GaAs substrate was grown with identical growth conditions for comparison purpose. Fig 10(a) shows the schematic diagram of the whole microdisk laser structure. For the fabrication of microdisk lasers, the 4 $\mu$m-diameter silica beads acted as the hard mask for the standard inductive coupled plasma (ICP) etching, followed by subsequent wet etching process. After removal of silicon beads, the microdisk lasers were achieved with a diameter of 4 $\mu$m. Fig. 10(b) shows the schematic diagram of a microdisk laser. Figs. 10(c) and 10(d) present the tilted SEM images of microdisk lasers on GaAs (001) and GaAs/Si (001) substrates, respectively. Both disk structures show vertical profile, smooth sidewall. The microdisk lasers on GaAs and Si (001) substrates are both characterized in the following part.

The microdisk lasers on GaAs and Si (001) substrate were measured under a micro-PL system with 532 nm-continuous-wave semiconductor laser. Figs. 11(a) and 11(c) show the integrated intensity of microdisk lasers versus the pump power

(L–L curve) on GaAs substrate and Si (001) substrate, respectively. The laser on Si (001) substrate has a pump power threshold as low as 380 $\mu$W, which is almost the same as that (330 $\mu$W) of the lasers on GaAs substrate. Typical 'S-shaped' nonlinear transition are shown both clearly in the insets of Figs. 11(a) and 11(c), including all three regimes of opeartion: spontaneous emission, amplified spontaneous emission and laser oscillation[64].

Figs. 11(b) and 11(d) show the lasers' spectra of the devices on GaAs and Si (001) substrate under different pump power. From the spectra, a high cavity quality factor (*Q*) of 3674 is obtained for the InAs QD lasers on Si (001) substrate, which is a little larger than that (3550) on GaAs substrate. Here, the higher *Q*-factor of microdisk on Si (001) substrate might result from the underneath grating-like Si patterns. The spacing of 17 and 18 nm between the adjacent modes in the same radial-order on GaAs substrate and Si (001) substrate, are obtained, respectively, agreeing well with the calculation result. In conclusion, high-performance O-band InAs QD microdisk lasers are achieved on CMOS-compatible Si (001) substrates, which show great pontetial as a light source in the integration of optoelectronic devices.

## 4. Summary and outlook

In conclusion, we have reported recent progress of hybrid epitaxially grown InAs QD microcavity lasers on (111)-faceted Si (001) substrates. A novel (111)-faceted Si (001) hollow substrate was invented to obtain defect-free, APB-free, and thermal crack-free III–V photonic structures on Si (001) platforms. High-efficient O-band and C/L band emission of InAs QDs were achieved on Si (001) substrates. In addition, high-performance O-band microdisk lasers were realized and characterized on the (111)-faceted Si (001) hollow substrates. Here, this hybrid epitaxial growth technique will provide a promising approach to migrate III–V optoelectronic materials on Si platforms for the future silicon photonics integration.

## Acknowledgments

The financial support was provided by the National Natural Science Foundation of China (Nos. 61635011, 11574356, 11434010, 61804177 and 11804382); National Key Research and Development Program of China (Nos. 2016YFA0300600 and 2016YFA0301700); Key Research Program of Frontier Sciences, CAS (No. QYZDB-SSW-JSC009); Ting Wang was supported by the Youth Innovation Promotion Association of CAS (No. 2018011).

## References

[1] Asghari M, Krishnamoorthy A V. Silicon photonics: Energy-efficient communication. Nat Photonics, 2011, 5(5), 268

[2] Rickman A. The commercialization of silicon photonics. Nat Photonics, 2014, 8(8), 579

[3] Vahdat A, Liu H, Zhao X, et al. The emerging optical data center. Optical Fiber Communication Conference, 2011, OTuH2

[4] Bauters J F, Davenport M L, Heck M J R, et al. Silicon on ultra-low-loss waveguide photonic integration platform. Opt Express, 2013, 21(1), 544

[5] Heck M J R, Bauters J F, Davenport M L, et al. Ultra-low loss waveguide platform and its integration with silicon photonics. Laser Photonics Rev, 2014, 8(5), 667

[6] Yin T, Cohen R, Morse M M, et al. 31 GHz Ge n–i–p waveguide photodetectors on silicon-on-insulator substrate. Opt Express, 2007, 15(21), 13965

[7] Vivien L, Polzer A, Marris-Morini D, et al. Zero-bias 40 Gbit/s germanium waveguide photodetector on silicon. Opt Express, 2012, 20(2), 1096

[8] Reed G T, Mashanovich G, Gardes F Y, et al. Silicon optical modulators. Nat Photonics, 2010, 4(8), 518

[9] Xiao X, Xu H, Li X, et al. High-speed, low-loss silicon Mach-Zehnder modulators with doping optimization. Opt Express, 2013, 21(4), 4116

[10] Zheng X, Shubin I, Li G, et al. A tunable 1 × 4 silicon CMOS photonic wavelength multiplexer/demultiplexer for dense optical interconnects. Opt Express, 2010, 18(5), 5151

[11] Liang D, Bowers J E. Recent progress in lasers on silicon. Nat Photonics, 2010, 4(8), 511

[12] Rong H, Liu A, Jones R, et al. An all-silicon Raman laser. Nature, 2005, 433(7023), 292

[13] Camacho-Aguilera R E, Cai Y, Patel N, et al. An electrically pumped germanium laser. Opt Express, 2012, 20(10), 11316

[14] Liu J, Sun X, Pan D, et al. Tensile-strained, n-type Ge as a gain medium for monolithic laser integration on Si. Opt Express, 2007, 15(18), 11272-11277

[15] Liu A Y, Bowers J. Photonic integration with epitaxial III–V on silicon. IEEE J Sel Top in Quantum Electron, 2018, 24(6), 1

[16] Tanabe K, Watanabe K, Arakawa Y. III–V/Si hybrid photonic devices by direct fusion bonding. Sci Rep, 2012, 2, 349

[17] Wang Z, Van Gasse K, Moskalenko V, et al. A III–V-on-Si ultra-dense comb laser. Light: Sci Appl, 2017, 6(5), e16260

[18] Zhou Z, Yin B, Michel J. On-chip light sources for silicon photonics. Light: Sci Appl, 2015, 4(11), e358

[19] Wang Z, Abbasi A, Dave U, et al. Novel light source integration approaches for silicon photonics. Laser Photonics Rev, 2017, 11(4), 1700063

[20] Liu C W, Östling M, Hannon J B. New materials for post-Si computing. MRS Bulletin, 2014, 39(8), 658

[21] Wu J, Chen S, Seeds A, et al. Quantum dot optoelectronic devices: lasers, photodetectors and solar cells. J Phys D, 2015, 48(36), 363001

[22] Tang M, Chen S, Wu J, et al. 1.3-$\mu$m InAs/GaAs quantum-dot lasers monolithically grown on Si substrates using InAlAs/GaAs dislocation filter layers. Opt Express, 2014, 22(10), 11528

[23] Wang J, Hu H Y, Deng C, et al. Defect reduction in GaAs/Si film with InAs quantum-dot dislocation filter grown by metalorganic chemical vapor deposition. Chin Phys B, 2015, 24(2), 028101

[24] Li Q, Lau K M. Epitaxial growth of highly mismatched III–V materials on (001) silicon for electronics and optoelectronics. Prog Cryst Growth Charact Mater, 2017, 63(4), 105

[25] Faucher J, Masuda T, Lee M L. Initiation strategies for simultaneous control of antiphase domains and stacking faults in GaAs solar cells on Ge. J Vac Sci Technol B, 2016, 34(4), 041203

[26] Liao M, Chen S, Park J S, et al. III–V quantum-dot lasers monolithically grown on silicon. Semicond Sci Technol, 2018, 33(12), 123002

[27] Brammertz G, Mols Y, Degroote S, et al. Low-temperature photoluminescence study of thin epitaxial GaAs films on Ge substrates. J Appl Phys, 2006, 99(9), 093514

[28] Alcotte R, Martin M, Moeyaert J, et al. Epitaxial growth of antiphase boundary free GaAs layer on 300 mm Si (001) substrate by metalorganic chemical vapour deposition with high mobility. Appl Mater, 2016, 4(4), 046101

[29] Akiyama M, Kawarada Y, Kaminishi K. Growth of single domain GaAs layer on (100)-oriented Si substrate by MOCVD. Jpn J Appl Phys, 1984, 23(11A), L843

[30] Chadi D J. Stabilities of single-layer and bilayer steps on Si (001) surfaces. Phys Rev Lett, 1987, 59(15), 1691

[31] Wang T, Liu H, Lee A, et al. 1.3-$\mu$m InAs/GaAs quantum-dot lasers monolithically grown on Si substrates. Opt Express, 2011, 19(12), 11381
[32] Lee A, Jiang Q, Tang M, et al. Continuous-wave InAs/GaAs quantum-dot laser diodes monolithically grown on Si substrate with low threshold current densities. Opt Express, 2012, 20(20), 22181
[33] Liao M, Chen S, Huo S, et al. Monolithically integrated electrically pumped continuous-wave III–V quantum dot light sources on silicon. IEEE J Sel Top Quantum Electron, 2017, 23(6), 1
[34] Chen S, Liao M, Tang M, et al. Electrically pumped continuous-wave 1.3 $\mu$m InAs/GaAs quantum dot lasers monolithically grown on on-axis Si (001) substrates. Opt Express, 2017, 25(5), 4632
[35] Norman J, Kennedy M J, Selvidge J, et al. Electrically pumped continuous wave quantum dot lasers epitaxially grown on patterned, on-axis (001) Si. Opt Express, 2017, 25(4), 3927
[36] Volz K, Beyer A, Witte W, et al. GaP-nucleation on exact Si (001) substrates for III/V device integration. J Cryst Growth, 2011, 315(1), 37
[37] Liu A Y, Peters J, Huang X, et al. Electrically pumped continuous-wave 1.3 $\mu$m quantum-dot lasers epitaxially grown on on-axis (001) GaP/Si. Opt Lett, 2017, 42(2), 338
[38] Jung D, Zhang Z, Norman J, et al. Highly reliable low-threshold InAs quantum dot lasers on on-axis (001) Si with 87% injection efficiency. ACS Photonics, 2017, 5(3), 1094
[39] Kwoen J, Jang B, Lee J, et al. All MBE grown InAs/GaAs quantum dot lasers on on-axis Si (001). Opt Express, 2018, 26(9), 11568
[40] Yang V K, Groenert M, Leitz C W, et al. Crack formation in GaAs heteroepitaxial films on Si and SiGe virtual substrates. J Appl Phys, 2003, 93(7), 3859
[41] Wei W Q, Wang J H, Gong Y, et al. C/L-band emission of InAs QDs monolithically grown on Ge substrate. Opt Mater Express, 2017, 7(8), 2955
[42] Wei W Q, Wang J H, Zhang B, et al. InAs QDs on (111)-faceted Si (001) hollow substrates with strong emission at 1300 nm and 1550 nm. Appl Phys Lett, 2018, 113(5), 053107
[43] Feng Q, Wei W, Zhang B, et al. O-band and C/L-band III–V quantum dot lasers monolithically grown on Ge and Si substrate. Appl Sci, 2019, 9(3), 385
[44] Liu H, Wang T, Jiang Q, et al. Long-wavelength InAs/GaAs quantum-dot laser diode monolithically grown on Ge substrate. Nat Photonics, 2011, 5(7), 416
[45] Kaspar P, Brenot R, Le Liepvre A, et al. Packaged hybrid III–V/silicon SOA. The European Conference on Optical Communication (ECOC), 2014, 1
[46] Ledentsov N N, Kovsh A R, Zhukov A E, et al. High performance quantum dot lasers on GaAs substrates operating in 1.5 $\mu$m range. Electron Lett, 2003, 39(15), 1126
[47] Wang T, Lee A, Tutu F, et al. The effect of growth temperature of GaAs nucleation layer on InAs/GaAs quantum dots monolithically grown on Ge substrates. Appl Phys Lett, 2012, 100(5), 052113
[48] Lee A, Liu H, Seeds A. Semiconductor III–V lasers monolithically grown on Si substrates. Semicond Sci Technol, 2012, 28(1), 015027
[49] Lee A D, Jiang Q, Tang M, et al. InAs/GaAs quantum-dot lasers monolithically grown on Si, Ge, and Ge-on-Si substrates. IEEE J Sel Top Quantum Electron, 2013, 19(4), 1901107
[50] Liu A Y, Zhang C, Norman J, et al. High performance continuous wave 1.3 $\mu$m quantum dot lasers on silicon. Appl Phys Lett, 2014, 104(4), 041104
[51] Chen S, Li W, Wu J, et al. Electrically pumped continuous-wave III–V quantum dot lasers on silicon. Nat Photonics, 2016, 10(5), 307
[52] Wan Y, Li Q, Geng Y, et al. InAs/GaAs quantum dots on GaAs-on-V-grooved-Si substrate with high optical quality in the 1.3 $\mu$m band. Appl Phys Lett, 2015, 107(8), 081106
[53] Wan Y, Li Q, Liu A Y, et al. Temperature characteristics of epitaxially grown InAs quantum dot micro-disk lasers on silicon for on-chip light sources. Appl Phys Lett, 2016, 109(1), 011104
[54] Li Q, Ng K W, Lau K M. Growing antiphase-domain-free GaAs thin films out of highly ordered planar nanowire arrays on exact (001) silicon. Appl Phys Lett, 2015, 106(7), 072105
[55] Shi B, Zhu S, Li Q, et al. Continuous-wave optically pumped 1.55 $\mu$m InAs/InAlGaAs quantum dot microdisk lasers epitaxially grown on silicon. ACS Photonics, 2017, 4(2), 204
[56] Shi B, Zhu S, Li Q, et al. 1.55 $\mu$m room-temperature lasing from subwavelength quantum-dot microdisks directly grown on (001) Si. Appl Phys Lett, 2017, 110(12), 121109
[57] Zhu S, Shi B, Wan Y, et al. 1.55 $\mu$m band low-threshold, continuous-wave lasing from InAs/InAlGaAs quantum dot microdisks. Opt Lett, 2017, 42(4), 679
[58] Wan Y, Jung D, Shang C, et al. Low-threshold continuous-wave operation of electrically pumped 1.55 $\mu$m InAs quantum dash microring lasers. ACS Photonics, 2018, 6(2), 279
[59] Zhang B, Wei W Q, Wang J H, et al. 1310 nm InAs quantum-dot microdisk lasers on SOI by hybrid epitaxy. Opt Express, 2019, 27(14), 19348
[60] McCall S L, Levi A F J, Slusher R E, et al. Whispering-gallery mode microdisk lasers. Appl Phys Lett, 1992, 60(3), 289
[61] Wan Y, Li Q, Liu A Y, et al. Optically pumped 1.3 $\mu$m room-temperature InAs quantum-dot micro-disk lasers directly grown on (001) silicon. Opt Lett, 2016, 41(7), 1664
[62] Li Q, Wan Y, Liu A Y, et al. 1.3-$\mu$m InAs quantum-dot micro-disk lasers on V-groove patterned and unpatterned (001) silicon. Opt Express, 2016, 24(18), 21038
[63] Wan Y, Norman J, Li Q, et al. 1.3 $\mu$m submilliamp threshold quantum dot micro-lasers on Si. Optia, 2017, 4(8), 940
[64] Siegman A E. Lasers. University Science Books, Mill Valley, CA, 1986